

Effects of atoms and molecules adsorption on electronic and magnetic properties of s-triazine with embedded Fe atom: DFT investigations

Yusuf Zuntu Abdullahi¹, Tiem Leong Yoon², Mohd Mahadi Halim³, Md.
Roslan Hashim⁴, and Thong Leng Lim⁵

¹*School of Physics, Universiti Sains Malaysia, 11800 Penang, Malaysia*

¹*Department of Physics, Faculty of Science, Kaduna State University, P.M.B.
2339 Kaduna State, Nigeria*

**E-mail: yusufzuntu@gmail.com (corresponding author)*

²*School of Physics, Universiti Sains Malaysia, 11800 Penang, Malaysia*

**E-mail: tlyoon@usm.my*

³*School of Physics, Universiti Sains Malaysia, 11800 Penang, Malaysia*

⁴*Institute of Nano-Optoelectronics Research and Technology Laboratory,
Universiti Sains Malaysia, 11900 Penang, Malaysia*

⁵*Faculty of Engineering and Technology, Multimedia University, Jalan Ayer
Keroh Lama, 75450 Melaka, Malaysia*

.....
In this paper we employ first-principles calculations to study the mechanical, geometrical, electronic and magnetic properties of Fe atom embedded *s*-triazine (Fe-C₆N₆) system under the influence of external environment. Our result show that the binding energy of Fe-C₆N₆ can be modulated by an applied tensile deformation and perpendicular electric field. The non-magnetic semiconducting property of pure *s*-triazine sheet (C₆N₆) is found to changed upon embedding of Fe atom in the porous site of the sheet. It is reveals that the Fe-C₆N₆ system exhibit half-metallic electronic character with magnetic moment which is in order of the value for an isolated Fe atom. Furthermore, electronic and magnetic properties of the Fe-C₆N₆ systems are preserved under a maximum value of 10 V/nm in electric field strength and 6% tensile strain. Interestingly, We find that the semiconducting electronic character and magnetic moment of Fe-C₆N₆ system can be tuned into semiconductor with low or high magnetic moment via adsorption of atoms C, N, O, H and molecules (CH₄, N₆, O₂, H₂, CO, CO₂) into Fe-C₆N₆ system. The appearance of semiconducting character is as a result of shift in impurity state towards higher energy when the atoms or molecules are adsorbed on Fe-C₆N₆ surface. Our findings may serve as a guide for future applications of Fe-C₆N₆ structures in spintronics devices.

1 Introduction

Currently there is an intense search for suitable substrates for transition metal (TM) atoms encapsulation [1-3]. The central point in the encapsulation is to ensure that the substrate remains inert and strongly binds to the TM atoms. Moreover, the appropriate substrate is expected to preserve its intrinsic properties and that of bound TM atoms. Two-dimensional (2D) carbon-based and related surfaces with compacted hexagonal rings have been the most frequent choice for trapping TM atoms [4-7]. This is due to their wide surface area. Numerous works have so far been done to investigate the stable geometries and electronic properties of TM atoms adsorption on graphene and boron nitride sheets [7-9]. However, their reports have shown that the adatoms tightly on these 2D surfaces as a result of low adsorption energies. Additionally, the large surface free energy of the TM atoms would make them aggregate easily to form cluster on these surfaces. To ensure the immobility of the TM atoms on the surface, various defects sites have been proposed [8]. Although creation of defects sites would presumably bind the TM atoms firmly on a surface. However, forming a regular defect sites experimentally may not be possible due to influence of external environment. Thus, more research efforts have been made to synthesis 2D materials with inherently defined porous sites [10].

Among the recently synthesized porous 2D materials [11], graphitic carbon nitride (CN) sheet has received much attention [12, 13]. This is due to its potentials as a right candidate for various applications [14-18]. Graphitic CN belongs to a group of allotrope with a common chemical formula $g-C_xN_y$, where x and y represent the number of C and N atoms in the unit cell. For example, graphitic single triazine-based has a chemical formula $g-s-C_3N_4$ whereas graphitic tri-single triazine-based (heptazine) is named $g-t-s-C_3N_4$ [13]. The hexagonal rings in the unit cell of heptazine are compacted in abreast manner. s -triazine with a chemical formula $g-C_6N_6$ is another allotrope of graphitic CN in which two of its hexagonal rings ($g-C_3N_3$) are separated via C-C bond [12]. Depending on the composition of C and N in the hexagonal rings and unit cell, these allotropes can have different electronic properties ranging from semiconducting to half-metallic. For instance, triazine-based $g-C_4N_3$ is another allotrope of graphitic CN which possess a ferromagnetic ground state with half metallic electronic character [19] whereas the rest of the allotropes are non-magnetic with wide or small band gaps [12, 13].

To search for a suitable spintronic material such as diluted magnetic semiconductor, first-principles calculations of TM atoms embedded in semi-conducting CN sheet have been performed [1-3]. Choudhuri *et al.* recently reported the findings of TM embedded $g-C_3N_3$ (TM@ $g-C_3N_3$) systems based on density functional theory (DFT) [20]. The TM atoms (Cr,

Mn and Fe) embedded g -C₃N₃ systems are found to be dynamical, thermally and mechanically stable. Their report also show that the Cr, Mn and Fe embedded in the g - t -C₃N₃ systems exhibit high temperature ferromagnetism and high magnetic anisotropy energy (MAE) with a peak value per atom occurring in Cr@ g - t -C₃N₃. It was also shown in our work that the band gap of Mn embedded heptazine system enhances under small tensile deformation whereas the magnetic moment of the system remains unperturbed under the same symmetric deformation [1].

TM embedded graphitic carbon nanostructures can also be used for heterogeneous catalysis, hydrogenation of CO₂ and as membrane for separation of gases [21-25]. A recent theoretical study predicts excellent catalytic activities for single atomic crystal (SAC) of TM embedded C₂N systems [24]. Additionally, an effective catalysis of hydrogenation of CO₂ into methanol on the copper embedded graphene system is demonstrated by Sirijaraensre and Limtrakul [25]. Although good catalytic behavior has been reported for the SAC of TM embedded C₂N systems, the comprehensive understanding of various types of atoms and molecules adsorbed onto their surfaces is still lacking. Thus, in this work, we investigate the structural, electronic and magnetic properties of Fe embedded s -triazine sheet with various adsorbed atoms and molecules. We begin by analyzing the Fe embedded s -triazine without the adsorbed atoms and molecules. Then, we introduce these (C,N,O,H) atoms and molecules (CH₄, N₂, O₂, H₂, CO, CO₂) above the porous site where Fe is situated at a distant height. The relaxed Fe embedded s -triazine with adsorbed atoms and molecules systems are used for further analysis.

2 Computational method

We use Quantum Espresso package [26] to carry out spin-polarised DFT [27] based on first-principles calculations within generalized gradient approximation of Perdew-Burke-Ernzerhof (PBE) approximations [28]. The Ultrasoft pseudopotentials method is employed to treat the core and valence electrons of C, N, and Fe (semi-core included) atoms [29]. A plain wave basis set with kinetic energy cut-off of 550 eV was used to expand the wave functions. We use Marzari-Vanderbilt smearing method with Gaussian spreading is employed [30] to aid the convergences of our systems. The Brillouin zone (BZ) is sampled with 881 and 15151 Monkhorst-Pack k-point meshes for the self-consistent field and density of state calculations respectively [31]. The planar sheet is treated with periodic boundary conditions and a thick vacuum space of 16 Å along the z -direction to avoid periodic layers' interaction. All geometries are fully relaxed using the BFGS quasi-Newton algorithm until Hellmann-Feynman force tolerance on each atom was smaller than 0.05 eV.

The optimized geometries of 2×2 pure *s*-triazine sheet (C_6N_6) and Fe embedded C_6N_6 sheet (Fe- C_6N_6) are displayed in Fig. 1 (a). All N atoms have sp^3 -like hybridized and each C atom which is bonded to three atoms is sp^2 -like hybridized structure. The relaxed C-C bond length d linking the *s*-triazine units in Fe- C_6N_6 system and C-N bond lengths l in the embedded Fe atom cavity are in the range 1.47-1.50 Å and 1.35-1.37 Å respectively. The calculated values agree well with the reported results [12]. The optimized lattice constant in the Fe- C_6N_6 is found to be 14.20 Å.

3 Results and Discussions

We used the expressions in Eq. (1) to compute the mechanical properties, such as in-plane stiffness Y (Young modulus), and Poisson ratio v :

$$\begin{aligned} Y &= m_{11} (1 - v^2) \\ v &= \frac{m_{12}}{m_{11}}. \end{aligned} \quad (1)$$

The variables m_{11} , m_{12} , (known as elastic constants) can be deduced from Eq. (2).

$$\begin{aligned} m_{11} &= \frac{1}{A_0} \left(\frac{\partial^2 E}{\partial s^2} \right) \Big|_{s=0} \quad (\text{uni - axial}) \\ 2(m_{11} + m_{12}) &= \frac{1}{A_0} \left(\frac{\partial^2 E}{\partial s^2} \right) \Big|_{s=0} \quad (\text{bi - axial}) \end{aligned} \quad (2)$$

where A_0 , E , and s are equilibrium unit-cell area, strain energy and applied deformation. At each 0.005 applied deformation (within the harmonic region for both bi- and uni-axial tensile strains, see Fig. 2) in the *xy*-plane, the structure is fully relaxed. The calculated in-plane stiffness is 1193.2 GPa·Å ($= 119.32 \text{ N/m}$), lower than the in-plane stiffness of pure heptazine sheets [13]. The Poisson's ratio 0.18 is in order of the value for graphene sheet [32]. The bulk modulus is determined from the product of equilibrium area and the second gradient of deformation energy with respect to area of the Fe- C_6N_6 system, which is written as

$$G = A \times \left(\frac{\partial^2 E}{\partial A^2} \right) \Big|_{A_m} \quad (3)$$

The variables in the Eq. (3) are defined as follows: A , U and A_m represent the area of the Fe- C_6N_6 sheet, the bi-axial deformation energy and the equilibrium area of Fe- C_6N_6 respectively. The calculated bulk modulus 86.49 N/m is less than the value for Mn-CN1 system reported in [1]. The difference in the calculated elastic constants in comparisons with previously related structures can be related to the weakening in the bonding networks of the

hexagonal rings in the structures. In Table 2 we show the values of binding energy E_b and the structural parameters h and d obtained for different deformations in the range $\pm 2\%$. By applying strain, the height h (difference between the height of Fe and the average height of all atoms in the C_6N_6 sheet) value of the Fe in the relaxed Fe- C_6N_6 sheet do not change. Hence, approximately zero h confirms the planar structure of the Fe- C_6N_6 sheet. The E_b is determined from the Eq. (4) which is given by:

$$E_b = (E_{\text{C}_6\text{N}_6} + E_{\text{Fe}}) - E_t \quad (4)$$

where E_t , $E_{\text{C}_6\text{N}_6}$ and E_{Fe} denote the total energy of Fe- C_6N_6 system, the energy of bare C_6N_6 sheet, and the total energy of an isolated Fe atom. The E_b for unstrained Fe- C_6N_6 system is equal to 4.73 eV. Our computed E_b value is consistent with the previous work [33]. It can also be seen that the Fe- C_6N_6 structure is more stable for positive binding energy and attained metastable state at a maximum 6% tensile strain. It is clearly shown in Table 2 that binding energy at a metastable state which is 6% tensile strain is found to be negative. The decrease in binding energy as a function of tensile strain can be explained as follows. Based on the definition of strain energy E (product of square of strain and the elastic constants) under harmonic deformations, an increasing E value stands for energetically favorable elastic moduli. Thus, for an increasing negative strain energy E of the Fe- C_6N_6 system (See Table 2), the binding energy according to Eq. (4) should correspondingly decreased. Table 2 illustrates the uniform increase in $d_{\text{Fe-N}}$ and d bond lengths as a result of distortion in the Fe- C_6N_6 structure caused by the tensile deformations.

It is known that the pure C_6N_6 sheet is non-magnetic semiconductor, thus the induced magnetism in the Fe- C_6N_6 system is mainly from Fe atom (see M_{Fe} in Table 2). For unstrained Fe- C_6N_6 system, the estimated magnetic moment per unit cell is 3.74 μ_B , which is consistent with recent report [33]. The magnetic moments are also evaluated for different applied tensile strain. It can be seen in Table 2 that the magnetic moment is less sensitive to the applied strain. This shows that the interaction between the Fe atom and the surrounding atoms in the porous site did not reduced the number of unpaired electrons in the d orbital of Fe atom. According to the Lowdin's charge analysis, the charge transfer Q into C_6N_6 sheet is contributed mainly by s, p orbitals of Fe atom. There is also a mixed bonding nature (ionic and covalent bonding) which is depicted in charge-density difference plot (see Fig. 1(c)) by charge depletion between the atoms and localisation around the most electronegative N atoms.

To analyze the electronic properties modulations of the Fe atom embedded s-triazine system, we plotted the electronic band structure and corresponding total and projected density of states. As can be clearly seen in Fig. 3(i), pure C_6N_6 is nonmagnetic semiconductor.

If Fe atom is embedded in the porous site of the C_6N_6 sheet, the electronic and magnetic properties are modulated. Fig. 4(a)-(f) show spin-polarised band structure, total density of states (TDOS) and corresponding projected density of state (PDOS) of Fe- C_6N_6 unstrained system. The figures portrays half metallic electronic character of Fe- C_6N_6 system. We can infer that the half-metallic character in Fe- C_6N_6 system is as a result of electron transfer from Fe sub-orbital induced by ionic interaction between the Fe and the C_6N_6 sheet. The minority band structure in Fig. 4 (a) confirms the half-metallic character which shows flat energy spectrum crossing over the fermi level at conduction band minimum. From the PDOS plots, we can observe a dominant features of Fe atom s-, d- sub-orbitals as well as small contributions by p_z - of the surrounding six N atom in the fermi level. At approximately -1.5 eV the bonding orbitals are contributed mainly by sp-like orbitals of the six N atoms, and the d_{xy} , $d_{x^2-y^2}$ orbitals of Fe atom in the majority spin state. Around -3.5 eV there is a mixed hybridization which is dominated by d-orbitals of the Fe atom in the majority spin state and s-, p_z -like orbitals of the surrounding N atoms in both majority and minority spin state.

The half-metallic electronic character and magnetic moment of Fe- C_6N_6 system under external environment i.e. symmetric tensile deformation by (up to 6% bi-axial tensile strain, see Table 2) and electric field (at a maximum of 10 V/nm, see Fig 3(iii)) are preserved. However, the binding of Fe atom in Fe- C_6N_6 enhances as more electric field strength are applied. The resulting higher energy of Fe- C_6N_6 system which corresponds to an increase E_b can be related to repulsive effect between the p_x , p_y orbitals of N atom and the d_{xy} , $d_{x^2-y^2}$ orbitals of Fe atom. This repulsion move p_z orbital towards higher energy and hence the system energy increases.

4 Adsorption of atoms and molecules on Fe embedded triazine sheet

The optimized stable geometries of Fe atom embedded *s*-triazine with adsorbed atoms C, N, O, H and molecules (CH_4 , N_2 , O_2 , H_2 , CO , CO_2) systems are displayed in Fig. 5 and 6. All atoms in the system are allowed to move freely without any constraint during the structural relaxation. We also listed the geometric parameters of the stable systems in Table 3. For the adsorbed atoms, the parameter h_{Fe-X} (where X represents atoms/molecules) are within chemisorption bonding height. These calculated bond lengths is an indications of interaction between embedded Fe atom and the adsorbed atoms. Nitrogen atom being the most electronegative has the shortest adsorption height and consequently due to strong interaction, the magnetic moment per unit cell is also the lowest. The estimated heights of h_{Fe-X} are in agreement with the recent work [24]. To determine the stability of the Fe- C_6N_6 with

adsorbed atoms/molecules systems, we calculate the adsorption energy which is expressed as

$$E_{\text{ads}} = (E_{\text{Fe-C}_6\text{N}_6} + E_x) - E_T \quad (5)$$

where E_T , $E_{\text{Fe-C}_6\text{N}_6}$ and E_x denotes the total energy of Fe-C₆N₆ with adsorbates, the energy of Fe-C₆N₆ system, and the total energy of an isolated atom or molecules respectively. Positive adsorption energy is an indication of a stable structure. The adsorption energies are listed in Table 3. The calculated results guarantee the chemical adsorption of all the systems.

As can be seen in Table 3, the adsorption of atoms on Fe-C₆N₆ sheet modulate the total magnetic moment per unit cell. The total magnetic moment in Fe-C₆N₆ with adsorbed O and H atoms systems increased whereas we find drastic magnetic moment reduction in Fe-C₆N₆ with adsorbed N and C systems. The modulation is related to the electron transfer between the Fe and the surrounding atoms. As illustrated in Table 3, the total magnetic moment is high where there are more charge transfer from Fe into the surrounding atoms as well as the adsorbed atoms H and O atoms). This shows that the interaction between Fe and O, H relatively preserved the number of unpaired in the d orbital of Fe. Thus, the atomic magnetic moment of Fe is maintained in those systems. In contrast, the Fe-C₆N₆ with adsorbed N or C atoms produces low spin configurations. TDOS of Fe-C₆N₆ with adsorbed atoms are depicted in Fig. 5. The TDOS Figures for Fe-C₆N₆ with adsorbed H and O show semiconductor electronic character whereas Fe-C₆N₆ with adsorbed C and N maintained hal-metallic character. The relative modulation of half-metallic character in Fe-C₆N₆ into semiconductor in Fe-C₆N₆ with adsorbed H and O is as caused by the shift in impurity state towards higher energy.

Next, we relaxed structures of Fe-C₆N₆ with six adsorbed molecules (CH₄, N₂, O₂, H₂, CO, CO₂). The stable adsorption height $h_{\text{Fe-X}}$, the corresponding adsorption energies and the bond lengths $d_{\text{avg-X}}$ of an isolated as well as adsorbed molecules are listed in Table 3. It can be seen that the adsorption heights vary slightly for different molecules. The smaller value of $h_{\text{Fe-X}}$ for adsorbed CO, O₂ and H₂ is an indication of favourable chemical bonding compared to other adsorbed molecules. Correspondingly, their $d_{\text{avg-X}}$ increases after chemisorption. Interestingly, the adsorption energies for CO and O₂ are almost the same. Our results is in disagreement with the recent report [24]. It was reported that O₂ would favourably chemisorbed on the Fe-C₆N₆ surface as compared to CO when the two gases are passed into the surface at constant pressure. Although we use DFT method in our ground state computations, the work in Ref. [24] employed DFT+*U* in the similar adsorption environment (different graphitic CN allotrope). We do not expect much difference in the computations of adsorption energy. However, our result is in order since the $h_{\text{Fe-X}}$ for

CO and O₂ are almost the same. It indicates strong interaction between CO, O₂ molecules and Fe atom due to hybridization. The computed adsorption energy for CO₂ is within the value suggested by Deng *et al.* [34].

As illustrated in Table 3, high magnetic moment per unit cell are obtained for different Fe-C₆N₆ with adsorbed molecules systems. As can be seen under M_{atom} , the contributions of the magnetic moment in the systems mainly originates from Fe atom. This shows that the high spin configuration of 3d electrons of the Fe atom are maintained. Except for CO and N₂ which couple antiferromagnetically with the Fe atoms, the rest of the molecules aligned in the same order with the Fe atom. Hence, the increased or decreased in the number of unpaired electrons in 3d of the Fe atom determines the total magnetic moment. Figs. 6 show the geometries and TDOS of Fe-C₆N₆ with adsorbed molecules. It can be seen that the half-metallic property of Fe-C₆N₆ system can be tuned to semiconducting property via adsorption of H₂, O₂ and CH₄ molecules on its surface.

5 Conclusion

In summary, we investigate the mechanical, geometrical, electronic and magnetic properties of Fe-C₆N₆ system under the influence of external environment based on first-principles calculations. Our findings reveal that the binding energy of Fe-C₆N₆ can be controlled by an applied tensile strain and perpendicular electric field. The non-magnetic semiconducting property of bare C₆N₆ is modulated upon embedding of Fe atom in the porous site of the sheet. It is found that the Fe-C₆N₆ system exhibit half-metallic electronic character with magnetic moment which is in order of the value for an isolated Fe atom. Additionally, the electronic and magnetic properties of the Fe-C₆N₆ systems are preserved under a maximum value of 10 V/nm in electric field strength and 6% tensile strain. Interestingly, We find that the semiconducting electronic character and magnetic moment of Fe-C₆N₆ system can be tuned into semiconductor and low/high magnetic moment restively via adsorption of atoms and molecules into Fe-C₆N₆ system. The appearance of semiconducting character is as a result of shift in impurity state towards higher energy when the atoms or molecules are adsorbed on Fe-C₆N₆ surface. Our findings may serve as a guide for future applications of Fe-C₆N₆ structures in spintronics devices.

Acknowledgments

T. L. Yoon wishes to acknowledge the support of Universiti Sains Malaysia RU grant (No. 1001/PFIZIK/811240). Figures showing atomic model and 2D charge-density difference plots

are generated using the XCRYSDEN program Ref. [35]. We gladly acknowledge Dr. Chan Huah Yong from the School of Computer Science, USM, for providing us computing resources to carry out part of the calculations done in this paper.

References

- [1] Y.Z. Abdullahi, T.L. Yoon, M.M. Halim, M.R. Hashim, M.Z.M. Jafri, L.T. Leng, *Curr. Appl. Phys.*, 16 (2016) 809.
- [2] S. Zhang, R. Chi, C. Li, Y. Jia, *Phys. Lett. A.*, 380 (2016) 1373.
- [3] D. Ghosh, G. Periyasamy, B. Pandey, S.K. Pati, *J. Mater. Chem. C.*, 2 (2014) 7943.
- [4] A. AlZahrani, *Physica B Condens Matter.*, 407 (2012) 992.
- [5] Y.Z. Abdullahi, M. Rahman, S. Abubakar, H. Setiyanto, *Quantum Matter*, 4 (2015) 430.
- [6] F. Ersan, . Arslanalp, G. Gkoğlu, E. Aktrk, *Appl. Surf. Sci.*, 371 (2016) 314.
- [7] M. Rahman, Y.Z. Abdullahi, A. Shuaibu, S. Abubakar, H. Zainuddin, R. Muhida, H. Setiyanto, *J. Comput. Theor. Nanosci.*, 12 (2015) 1995.
- [8] Z. Zhang, Z. Geng, D. Cai, T. Pan, Y. Chen, L. Dong, T. Zhou, *Physica E.*, 65 (2015) 24.
- [9] Y. Yagi, T.M. Briere, M.H. Sluiter, V. Kumar, A.A. Farajian, Y. Kawazoe, *Phys. Rev. B.*, 69 (2004) 075414.
- [10] E. Kroke, M. Schwarz, E. Horath-Bordon, P. Kroll, B. Noll, A.D. Norman, *New J. Chem.*, 26 (2002) 508.
- [11] M. Asadpour, S. Malakpour, M. Faghihnasiri, B. Taghipour, *Solid State Commun.*, 212, 46 (2015).
- [12] A. Wang, X. Zhang, M. Zhao, *Nanoscale* 6 (2014) 11157.
- [13] Y. Z. Abdullahi, T. L. Yoon, M. M. Halim, M. R. Hashim, T. L. Lim, *Solid State Commun.*, 248 (2016) 144.
- [14] Q.H. Wang, K. Kalantar-Zadeh, A. Kis, J.N. Coleman, M.S. Strano, *Nat. Nanotechnol.*, 7 (2012) 699.
- [15] X.-H. Li, X. Wang, M. Antonietti, *Chem. Sci.*, 3 (2012) 2170.
- [16] J. Zhang, M. Grzelczak, Y. Hou, K. Maeda, K. Domen, X. Fu, M. Antonietti, X. Wang, *Chem. Sci.*, 3 (2012) 443.
- [17] X. Zhang, X. Xie, H. Wang, J. Zhang, B. Pan, Y. Xie, *J. Am. Chem. Soc.*, 135 (2012) 18.
- [18] X. Zhang, H. Wang, H. Wang, Q. Zhang, J. Xie, Y. Tian, J. Wang, Y. Xie, *Adv. Mater.*, 26 (2014) 4438.
- [19] A. Du, S. Sanvito, S.C. Smith, *Phys. Rev. Lett.*, 108 (2012) 197207.

- [20] I. Choudhuri, P. Garg, B. Pathak, J. Mater. Chem. C., 4 (2016) 8253.
- [21] S. Sun, G. Zhang, N. Gauquelin, N. Chen, J. Zhou, S. Yang, W. Chen, X. Meng, D. Geng, M.N. Banis, Sci. Rep., 3 (2013).
- [22] Y. Ji, H. Dong, H. Lin, L. Zhang, T. Hou, Y. Li, RSC Adv., 6 (2016) 52377.
- [23] Z. Ma, X. Zhao, Q. Tang, Z. Zhou, Int. J. Hydrogen Energy., 39 (2014) 5037.
- [24] D. Ma, Q. Wang, X. Yan, X. Zhang, C. He, D. Zhou, Y. Tang, Z. Lu, Z. Yang, Carbon 105 (2016) 463.
- [25] Sirijaraensre, J., Limtrakul, J, Appl. Surf. Sci., 364 (2016) 241.
- [26] P. Giannozzi, S. Baroni, N. Bonini, M. Calandra, R. Car, C. Cavazzoni, D. Ceresoli, G.L. Chiarotti, M. Cococcioni, I. Dabo, J. Phys. Condens. Matter., 21 (2009) 395502.
- [27] P. Hohenberg, W. Kohn, Phys Rev., 136 (1964) B864.
- [28] J.P. Perdew, K. Burke, M. Ernzerhof, Phys. Rev. Lett., 77 (1996) 3865.
- [29] D. Vanderbilt, Phys. Rev. B., 41 (1990) 7892.
- [30] D. Vanderbilt, Phys. Rev. B., 41 (1990) 7892.
- [31] H.J. Monkhorst, J.D. Pack, Phys. Rev. B., 13 (1976) 5188.
- [32] E. Cadelano, P.L. Palla, S. Giordano, L. Colombo, Phys. Rev. B., 82 (2010) 235414.
- [33] K. Srinivasu, B. Modak, S.K. Ghosh, Phys. Chem. Chem. Phys., 18 (2016) 26466.
- [34] Q. Deng, L. Zhao, X. Gao, M. Zhang, Y. Luo, Y. Zhao, Small 9 (2013) 3506.
- [35] A. Kokalj, Computer. Mater. Sci., 28 (2003) 155.

Table 1 Calculated lattice parameters and total strain energy for Fe atom embedded striazine system.

Strain (%)	Area (\AA^2)	Total energy Biaxial (Ry)	Total energy Uniaxial (Ry)	Lattice parameter Biaxial (\AA)
-0.02	167.61	-998.95042	-998.98795	13.91/24.10
-0.015	169.32	-998.97718	-998.99904	13.98/24.22
-0.01	171.05	-998.99598	-999.00600	14.05/24.34
-0.005	172.78	-999.00762	-999.00946	14.13/24.47
0	174.52	-999.01171	-999.01171	14.20/24.59
0.005	176.27	-999.00880	-999.01108	14.27/24.71
0.01	178.03	-998.99980	-999.00779	14.34/24.83
0.015	179.79	-998.98403	-999.00136	14.41/24.96
0.02	181.57	-998.96248	-998.99209	14.48/25.08

Table 2 The calculated binding energies E_b , the average bond length between Fe atom and N_{edge} atoms $d_{\text{Fe-N}}$, average bond length connecting the s -triazine d , and Fe height h (refers to the difference in the z -coordinate of the Fe atom and the average of the z -coordinate of all the C and N atoms in the C_6N_6 sheet). Charge transfer, magnetic moment per unit cell and per Fe atom, electronic character of the Fe- C_6N_6 system are denoted by Q , M_{cell} , M_{Fe} , EC respectively. All the systems are half-metallic.

Strain	E_b (eV)	$d_{\text{Fe-N}}$ (\AA)	d (\AA)	h (\AA)	Q (electrons)	M_{Fe} (μ_B)	M_{cell} (μ_B)	EC
0%	4.73	2.06 – 3.40	1.49	-0.01	0.53	3.61	3.74	HM
1%	4.56	2.06 – 3.49	1.51	-0.01	0.54	3.61	3.73	HM
2%	4.05	2.09 – 3.56	1.53	0.00	0.56	3.61	3.71	HM
3%	3.21	2.09 – 3.64	1.55	0.00	0.56	3.61	3.70	HM
4%	2.06	2.02 – 3.80	1.58	0.00	0.53	3.57	3.69	HM
5%	0.75	2.08 – 3.82	1.61	0.00	0.54	3.57	3.66	HM
6%	-0.82	2.08 – 3.91	1.63	0.00	0.56	3.57	3.64	HM

Table 3 The calculated adsorption energy E_{ads} , $h_{\text{Fe}-X}$ refers to averaged height between Fe atom and the adsorbates. $d_{\text{avg}-X}$ denotes bond length of molecules. X represents adsorbate species. The values without parenthesis are that for absorbed molecules while that in parenthesis are for isolated molecules. Q refers to net charge transfer among the adsorbates and the Fe-C₆N₆ system. The values without parenthesis are charge transfer from Fe atom into the sheet or adsorbates. These values are all positive as electron from Fe atom always get transferred into the surrounding. The Q values in parenthesis are charge transfer into the Fe-striazine sheet from adsorbates. Positive values mean electron is transferred into the surroundings (Fe-C₆N₆ system) from adsorbates, and vice versa. M_{cell} refers to magnetic moment per unit cell. M_{atom} refers to magnetic moment of Fe atom or adsorbates. The values without parenthesis are that for Fe atom, while that in parenthesis are that for the adsorbates. EC refers to the electronic character of the Fe-C₆N₆ with adsorbates. In the present case, EC can be either half metallic (HM) or semiconducting (SC).

System	E_{ads} (eV)	$h_{\text{Fe}-X}$ (Å)	$d_{\text{avg}-X}$ (Å)	Q (electrons)	M_{cell} (μ_{B})	M_{atom} (μ_{B})	EC
C	4.48	1.56	-	0.13 (0.19)	1.68	2.17 (-0.71)	HM
N	3.00	1.52	-	0.24 (0.02)	1.56	1.53 (-0.12)	HM
O	4.11	1.65	-	0.54 (-0.34)	4.57	3.45 (0.78)	SC
H	1.90	1.60	-	0.46 (-0.12)	4.31	3.93 (0.11)	SC
CO	1.30	1.89	1.14 (1.16)	0.29 (C: 0.33, O: 0.09)	3.53	3.48 (-0.13)	SC
CO ₂	0.44	2.16	1.18 (1.18)	0.50 (C: 0.79, O: -0.41)	3.78	3.64 (0.24)	HM
O ₂	1.32	1.82	1.23 (1.40)	0.52 (-0.23)	3.70	3.12 (0.49)	HM
N ₂	0.15	2.12	1.11 (1.14)	0.36 (0.2)	3.55	3.51 (-0.15)	HM
H ₂	0.31	1.87	0.75 (0.79)	0.42 (0.21)	3.68	3.53 (0.00)	SC
CH ₄	0.18	2.16	1.10 (1.10)	0.51 (C: -0.64, H: 0.90)	3.76	3.62 (0.02)	SC

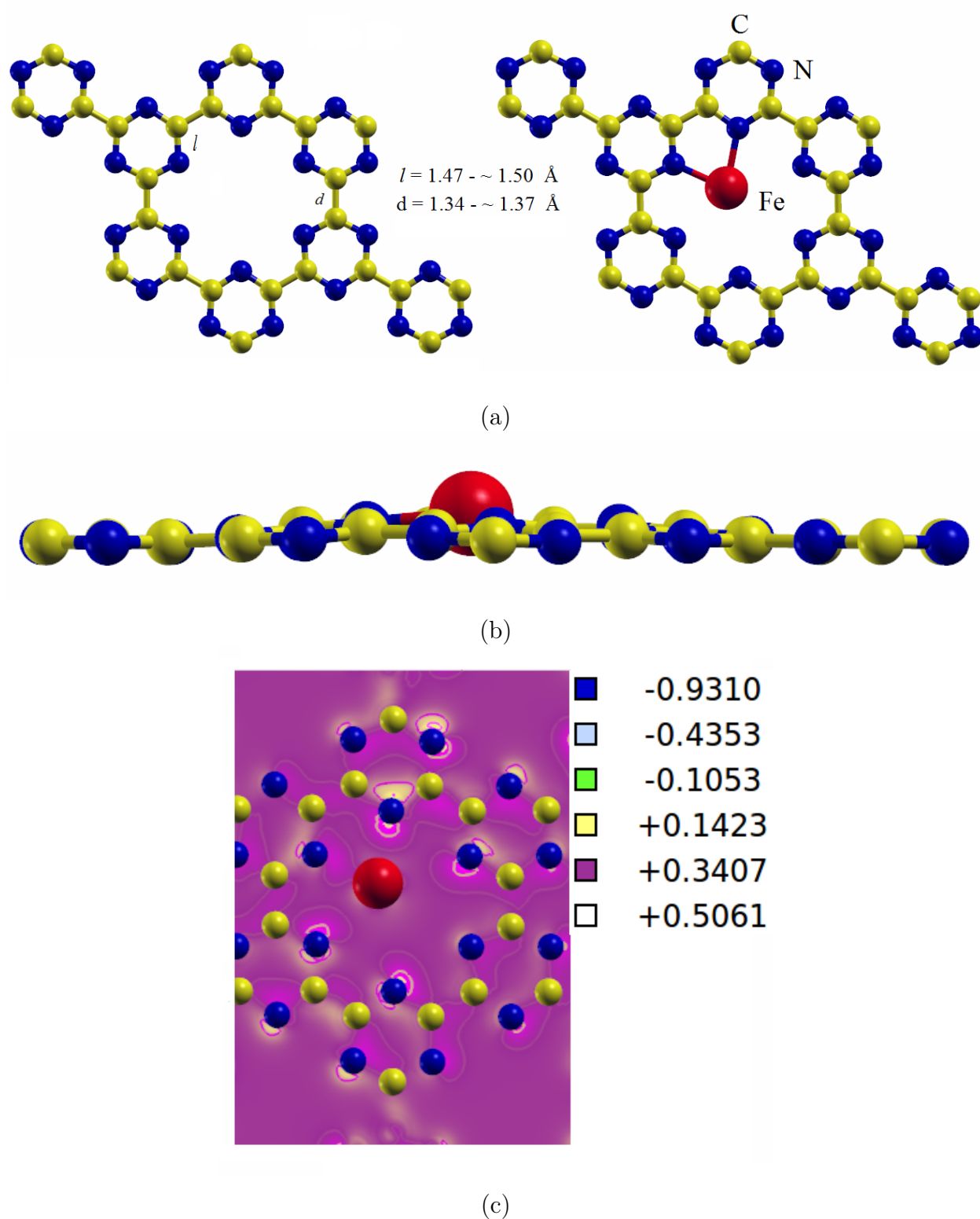


Figure 1 (a). Relaxed structure of 2×2 C₆N₆ sheet (Left panel) and relaxed structure (Right) of Fe embedded 2×2 C₆N₆. (b). Relaxed side view of 2×2 C₆N₆ sheet with an embedded Fe atom (Fe-C₆N₆) under perpendicular electric field strength of 10 V/nm. (c). Difference charge-density for Fe atom embedded *s*-triazine. The color scale shows ranges of charge accumulation and depletion in a.u.

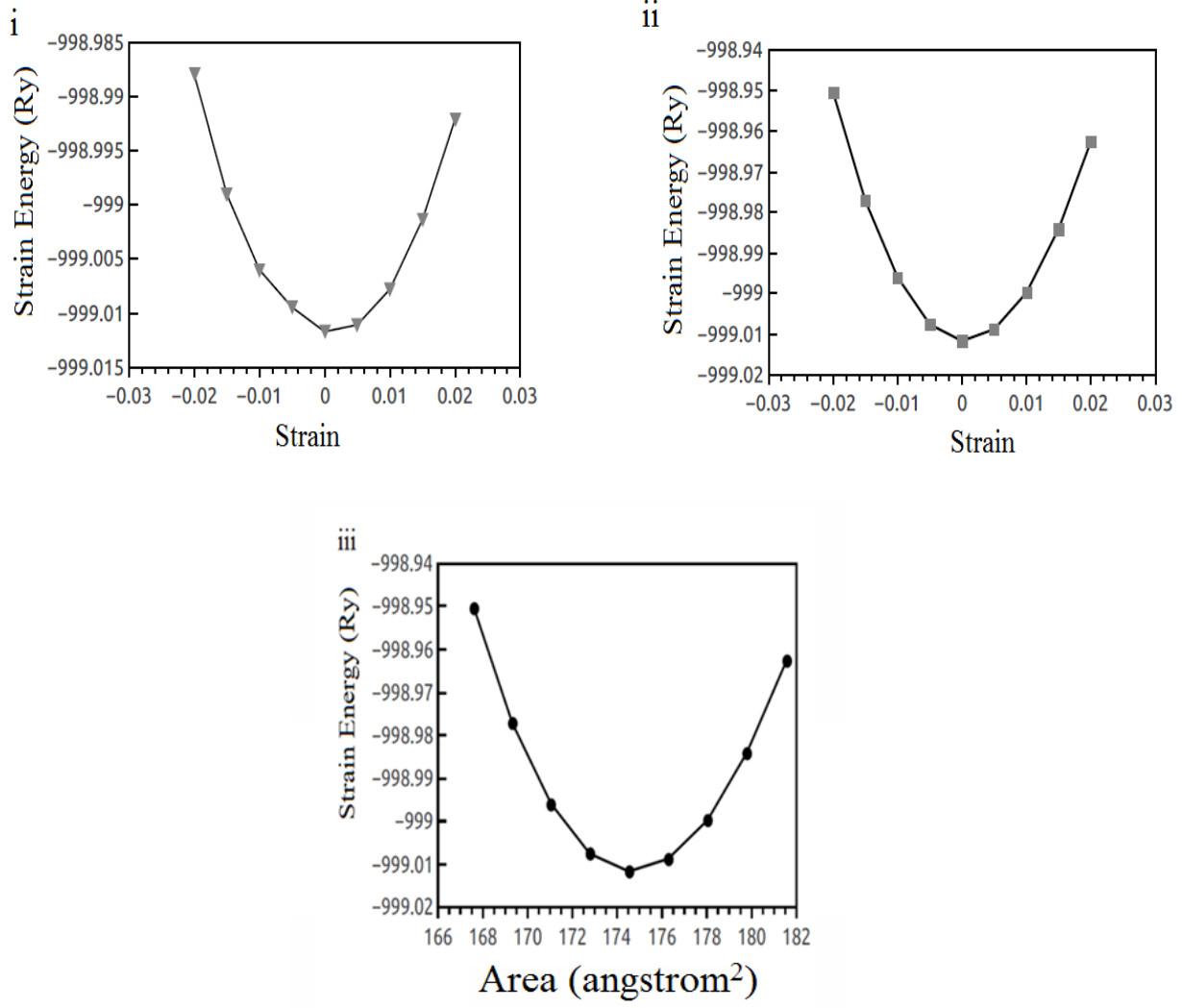


Figure 2 The variation of strain energy (Ry) versus (i) bi-axial tensile strain (ii) uni-axial tensile strain and (iii) area of the Fe-C₆N₆ system for elastic constant calculation.

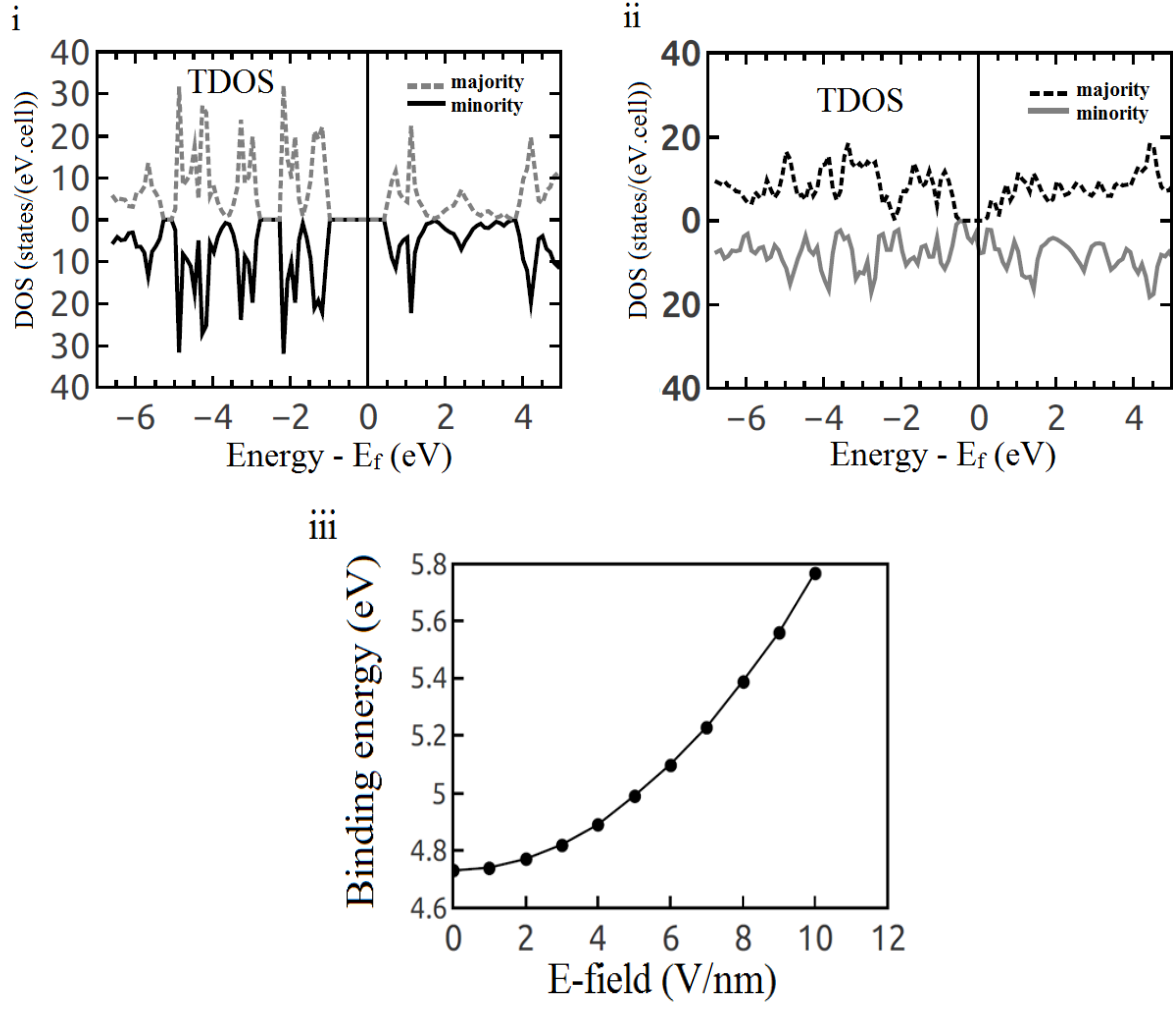


Figure 3 The spin-polarized total density of state (TDOS) for (i) pure s-triazine sheet (ii) Fe-C₆N₆ under applied electric field. (ii) Variation of binding energy versus applied electric field strength for Fe-C₆N₆ system.

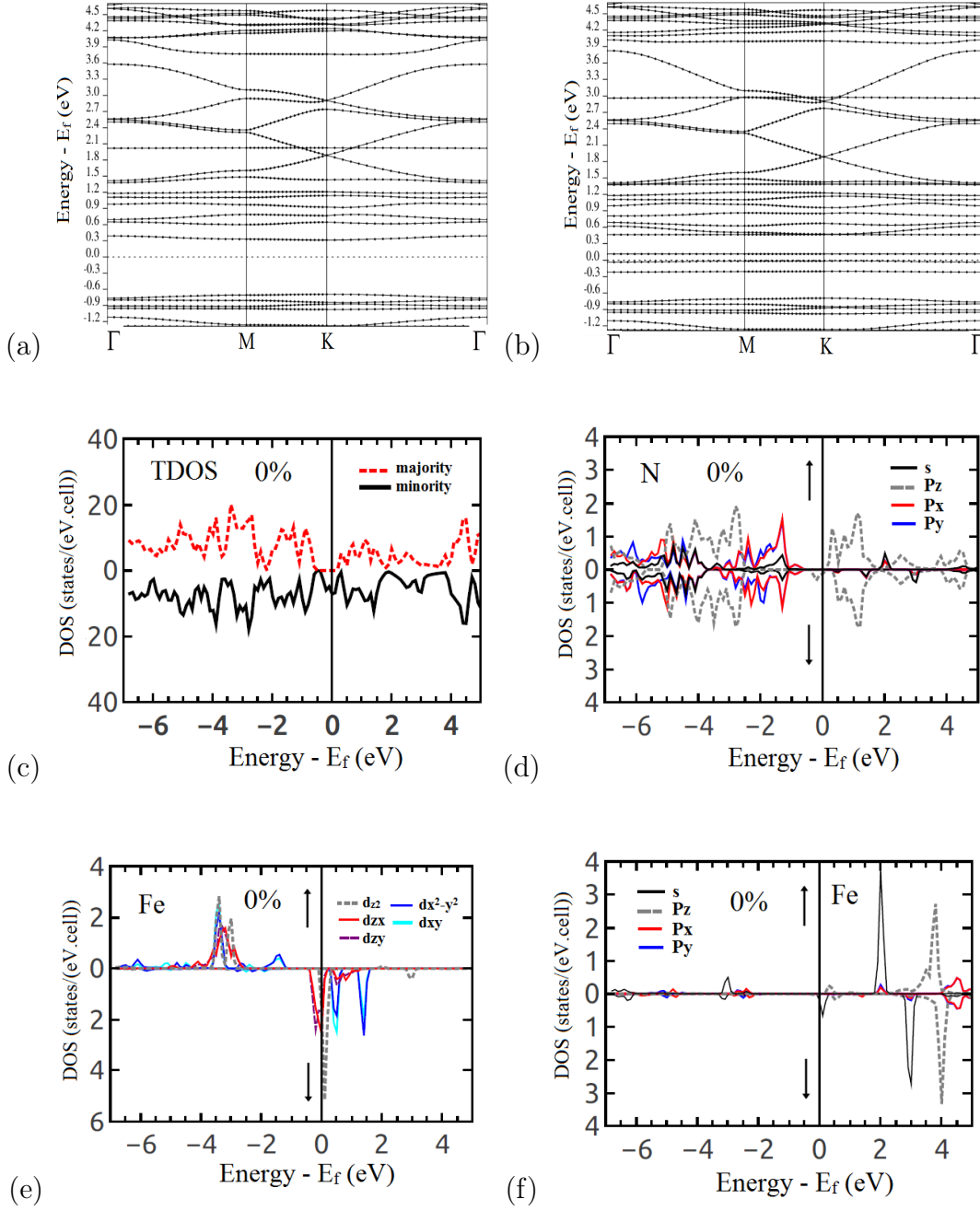


Figure 4 Spin-polarized electronic band structure (a) majority (b) minority spin states for unstrained ($s = 0$) Fe-C₆N₆ system. Spin-polarized TDOS and projected density of state (PDOS) for strain-free (c)-(f).

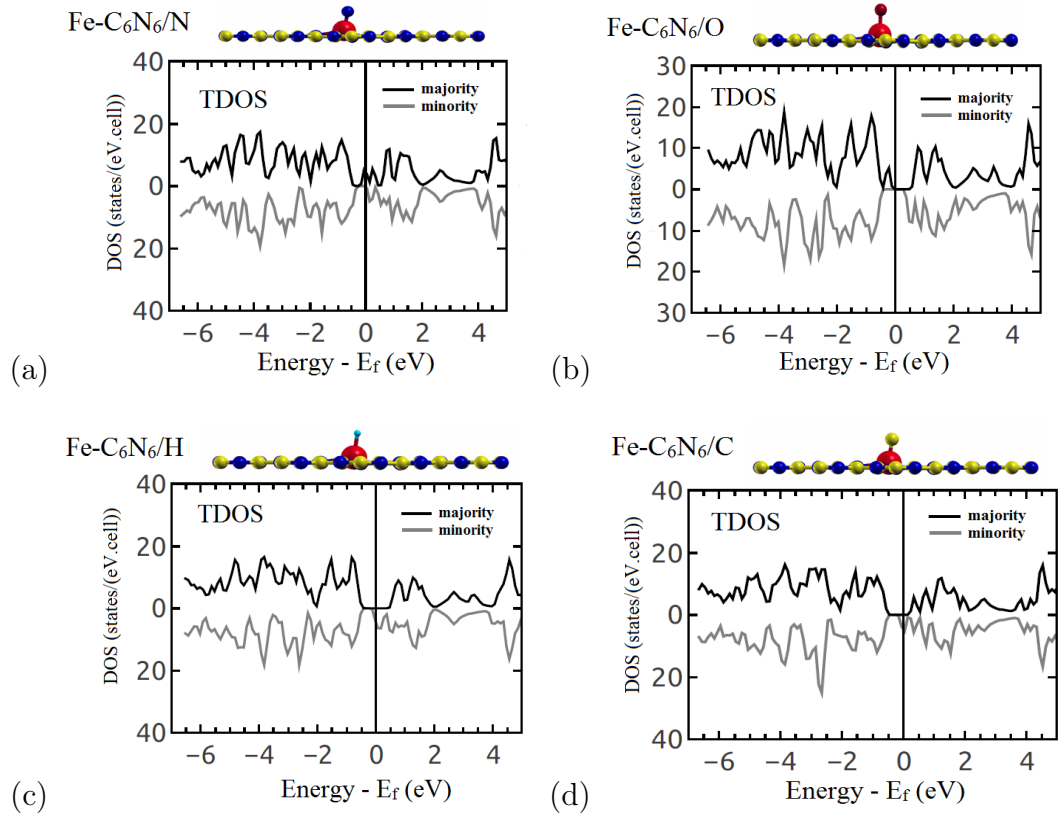


Figure 5 Spin-polarized TDOS and side view for Fe-C₆N₆ with an adsorbed (a) C (b) N (c) O and (d) H atoms systems respectively.

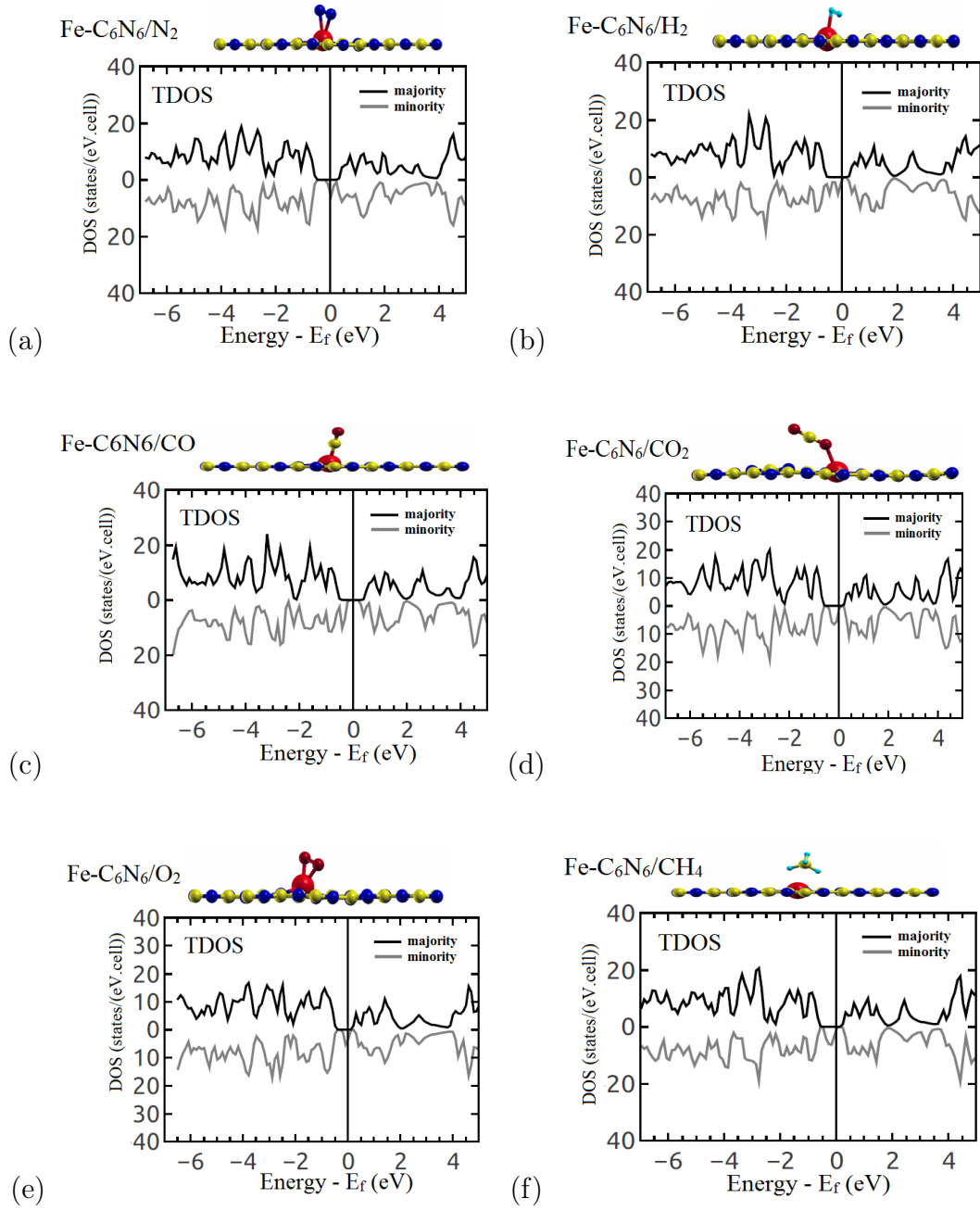


Figure 6 Spin-polarized TDOS and side view for Fe-C₆N₆ with an adsorbed (a) N₂ (b) H₂ (c) CO (d) CO₂ (e) O₂ and (f) CH₄ molecules systems respectively.